NASA Technical Memorandum 81477

PRESSURE SPECTRA AND CROSS SPECTRA AT AN AREA CONTRACTION IN A DUCTED COMBUSTION SYSTEM

J. H. Miles
Lewis Research Center
Cleveland, Ohio

and

D. D. Raftopoulos
University of Toledo
Toledo, Ohio

Prepared for the
1980 ASME Aerospace Conference
a part of the Century 2 Emerging Technology Conferences
San Francisco, California, August 13-15, 1980

at the NASA Lewis Research Center as part of a combustion noise research program. The analysis applies to a model previously developed in reference (1). This model was used in reference (1) to analyze auto-spectra measured in the long duct part of the facility shown in Fig. 1. The results indicated that the measured auto-spectra structure was affected by the presence of oxidizing soot particles which caused attenuation and dispersion. In this paper, in addition to analyzing the pressure auto-spectra on both sides of the area contraction, the model is used to analyze the pressure cross-spectra. Since the cross-spectra phase angles are dependent only on propagation effects, this comparison of model results and measurements provides an improved test of the model.

In the first part of this paper, the model is discussed. Next, the experimental results are presented. Last, the theoretical and experimental results are compared.

ANALYTICAL MODEL

The following assumptions are used in this analysis:

(1) Fluctuations in the gas of pressure, velocity, density, entropy, and temperature are assumed to be small compared with their equilibrium values so that their squares and cross products may be neglected.

(2) The bulk gas is a perfect gas.

(3) The soot particles are spherical, non-porous, and of a uniform temperature and size.

(4) The volumetric heat-transfer rate in a volume element containing a large number of soot particles is the sum of the effects due to each particle.

(5) Mass transfer and the body force due to viscous drag can be neglected.

In addition, the consequences of soot particle surface oxidation are idealized as producing a constant time-independent soot particle temperature. Moreover, waves propagating at the velocity of the flow are assumed to have negligible effects on pressure and particle velocity.

The one-dimensional continuity, momentum, and energy equations for the gas are:

$$\frac{\partial \bar{\rho}}{\partial t} + \frac{\partial}{\partial x}\left(\bar{\rho}\,\bar{u}\right) = 0 \tag{1}$$

$$\bar{\rho}\frac{D\bar{u}}{Dt} = -\frac{\partial \bar{p}}{\partial x} \tag{2}$$

$$\bar{\rho}\,\bar{t}\,\frac{D\bar{s}}{Dt} = n\left(4\pi r_s^2\right)\left(\frac{Nu_H}{d_s}\right)k\left(\bar{t}_s - \bar{t}\right) \tag{3}$$

where D/Dt is the substantial derivative $D/Dt = \partial/\partial t + u_o\,\partial/\partial x$.

Equations (1) to (3) are linearized by considering small perturbations of the variables from their equilibrium values. Substitution of the small perturbation form of the variables ρ, u, p, t, and s and elimination of squares and cross-products yields the following linearized equations written in non-dimensional form.

$$\frac{D}{Dt}\left(\frac{\rho_1}{\rho_o}\right) + c_o\,\frac{\partial}{\partial x}\left(\frac{u_1}{c_o}\right) = 0 \tag{4}$$

$$\frac{D}{Dt}\left(\frac{s_1}{c_p}\right) = -c_o\,\frac{\partial}{\partial x}\left(\frac{p_1}{\gamma p_o}\right) \tag{5}$$

$$\frac{D}{Dt}\left(\frac{s_1}{c_p}\right) = -\frac{\kappa_s}{\tau_s}\,\frac{t_{1,s}}{t_{o,s}} \tag{6}$$

where the particle mass fraction, κ_s, is a non-dimensional group of parameters defined as

$$\kappa_s = \frac{m_s}{\tau_s c_o} \tag{7}$$

and the heat-transfer time constant is defined as

$$\tau_s = \frac{m_s c_p}{\left(4\pi r_s^2\right)\left(\frac{Nu_H}{d_s}\right)k} \tag{8}$$

Equations (4) to (6) are simplified by using small perturbation thermodynamic relations. The ideal gas entropy equation is then

$$\frac{s_1}{c_p} = \frac{1}{\gamma}\frac{p_1}{p_o} - \frac{\rho_1}{\rho_o} \tag{9}$$

The gas equation of state

$$\bar{p} = \bar{\rho}\mathcal{R}\bar{t} \tag{10}$$

becomes

$$\frac{p_1}{p_o} = \frac{\rho_1}{\rho_o} + \frac{t_{1,s}}{t_{o,s}} \tag{11}$$

Equations (9) and (11) are next substituted into equation (6). Further the convective term of the substantial derivative in equation (6), $u(\partial s/\partial x)$, is neglected so that the final equations will have no modes propagating at the flow velocity. Thus

$$\frac{d}{dt}\left(\frac{s_1}{c_p}\right) = \frac{d}{dt}\left[\left(\frac{1-\gamma}{\gamma}\right)\frac{p_1}{p_o} + \frac{t_{1,s}}{t_{o,s}}\right] = -\frac{\kappa_s}{\tau_s}\,\frac{t_{1,s}}{t_{o,s}} \tag{12}$$

Consequently, the bulk gas temperature is related to the pressure by

$$\left(\frac{d}{dt} + \frac{\kappa_s}{\tau_s}\right)\frac{t_{1,s}}{t_{o,s}} = -\frac{d}{dt}\left(\frac{1-\gamma}{\gamma}\right)\frac{p_1}{p_o} \tag{13}$$

Taking the time Fourier transform of equations (12) and (13) yields the following transfer functions relating a perturbation in air temperature and entropy to a perturbation in pressure:

$$\Phi\left[\frac{t_{1,s}}{t_{o,s}}\right] = -\frac{(-i\omega)(1-\gamma)}{\left[(-i\omega) + \frac{\kappa_s}{\tau_s}\right]}\,\Phi\left[\frac{p_1}{\gamma p_o}\right] \tag{14}$$

$$\mathcal{F}\left[\frac{s_1}{c_p}\right] = \frac{S(\omega)}{c_p}\,\mathcal{F}\left[\frac{p_1}{\gamma p_o}\right] \tag{15}$$

where

$$\frac{S(\omega)}{c_p} = \frac{(1-\gamma)}{1 + (-i\omega)\frac{\ell_s}{\gamma_s}} \tag{16}$$

The time Fourier transform of equation (5) is

$$\left[(-i\omega) + u_o \frac{\partial}{\partial x}\right]\mathcal{F}\left[\frac{u}{c_o}\right] + c_o \frac{\partial}{\partial x}\,\mathcal{F}\left[\frac{p_1}{\gamma p_o}\right] = 0 \tag{17}$$

Taking the time Fourier transform of equation (4) after removing the density perturbation using equation (10) and then using equation (15) to remove the entropy perturbation yields

$$\left[(-i\omega) + u_o \frac{\partial}{\partial x}\right]\left[1 - \frac{S(\omega)}{c_p}\right]\mathcal{F}\left[\frac{1}{\gamma}\frac{p_1}{p_o}\right] + c_o \frac{\partial}{\partial x}\,\mathcal{F}\left[\frac{u_1}{c_o}\right] = 0 \tag{18}$$

A time Fourier transformed velocity potential solution of equations (17) and (18) is obtained next using

$$\mathcal{F}[u_1] = -\frac{\partial}{\partial x}\,\mathcal{F}[\Psi] \tag{19}$$

and

$$\mathcal{F}[p_1] = c_o\left[(-i\omega) + u_o \frac{\partial}{\partial x}\right]\mathcal{F}[\Psi] \tag{20}$$

Substituting equations (19) and (20) into equation (18) yields the following Fourier transformed velocity potential wave equation:

$$\left[(-ik_s) + M_s \frac{d}{dx}\right]^2 \mathcal{F}[\Psi] - \frac{d^2}{dx^2}\,\mathcal{F}[\Psi] = 0 \tag{21}$$

where

$$c_s = \frac{c_o}{\left[1 - S(\omega)/c_p\right]^{1/2}} \tag{22}$$

$$k_s = \omega/c_s \tag{23}$$

and

$$M_s = u_o/c_s \tag{24}$$

The velocity potential solution is assumed to be proportional to $\exp\left[(ik_o\Omega)^{\pm} - i\omega t\right]$. Substituting this solution into equation (21) yields a wave number equation which has as a solution:

$$(ik_o\Omega)^{+} = i(\omega/c_s)/(M_s + 1) \tag{25}$$

$$(ik_o\Omega)^{-} = -i(\omega/c_s)/(1 - M_s) \tag{26}$$

Consequently, the velocity potential wave equation solution consists of an acoustical wave travelling upstream and downstream which can be expressed in terms of a velocity potential function as

$$\Psi = \left[ae^{(ik_o\Omega)^{+}x} + be^{(ik_o\Omega)^{-}x}\right]e^{-i\omega t} \tag{27}$$

By definition, the propagation velocity is related to the wave number equation by

$$c(\omega) = \frac{\omega}{\mathrm{Im}(ik_o\Omega)},\ \mathrm{m/sec} \tag{28}$$

Also by definition, the acoustic attenuation coefficient in Nepers per meter is

$$\alpha = -2\mathrm{Re}(ik_o\Omega) \tag{29}$$

Nepers per meter is converted to decibels per meter by multiplying by 10. log e = 4.34

$$\alpha = -8.68\ \mathrm{Re}(ik_o\Omega),\ \mathrm{dB/m} \tag{30}$$

APPLICATION TO DUCTED COMBUSTION SYSTEM

The analysis developed in the last section is now used to study the spectral structure of pressure measurements made in the ducted combustion system shown in Fig. 1. The ducted combustion system shown in Fig. 1 consists of: (1) a source region inside the combustor can, (2) a non-source region inside a spool piece and a long duct, (3) an area expansion and contraction on either side of the spool piece, and (4) an upstream boundary at the exit of the long duct and a downstream boundary at the combustor inlet.

The solution for the velocity potential in a non-source region is given by equation (21). The Fourier transformed velocity potential wave equation (eq. (21)) is assumed to apply in the source region with the addition of a source term $G(\omega,x)$ on the right-hand side. Using the combustor inlet and exit impedance as a boundary condition, a unique Green's function solution for the Fourier transformed velocity potential is found. The Fourier transformed acoustic pressure and particle velocity can be found from a velocity potential using equations (19) and (20). Consequently, the acoustic pressure and particle velocity at the combustor exit can be determined from the velocity potential solution in the combustor. The acoustic pressure and particle velocity at the combustor exit can then be used to find the acoustic pressure and particle velocity at any other point in the ducted combustor system with four-pole equations in transfer matrix form derived using equations (19), (20), and (27). The combustor exit impedance can be calculated from the duct exit impedance using the same four-pole transfer matrix equations. The source region solution, duct transfer matrix, area discontinuity matrix, and boundary conditions are discussed in more detail in reference (1).

The following procedure is used to calculate the pressure spectrum. It is applied at each frequency as necessary to obtain the desired spectrum. First, the exit pressure perturbation is arbitrarily assumed to be one Pascal. Then using the duct exit acoustic impedance the particle velocity is calculated. Next,

using the duct transfer matrix and the area discontinuity transfer matrix as necessary, the acoustic state vector at the duct exit is used to find the acoustic state vector at the combustor exit. The resulting acoustic pressure and particle velocity are used to calculate the combustor exit impedance.

The next phase uses this impedance, the combustor entrance impedance, and a white noise source spectrum to determine the velocity potential solution in the source region. This velocity potential solution is used to calculate the acoustic pressure and particle velocity at the combustor exit due to the specified source and boundary conditions.

The last phase uses the duct transfer matrix and the area discontinuity matrix as necessary to calculate the acoustic state vector at any point in the duct from the acoustic state vector at the combustor exit. The pressure auto-spectrum at a given point is calculated from

$$H_{ii} = \overbrace{p_1^*(\omega,x_i)p_1(\omega,x_i)} \tag{31}$$

and the cross-spectrum between two points is calculated from

$$H_{ij} = \overbrace{p_1^*(\omega,x_i)p_1(\omega,x_j)} \tag{32}$$

EXPERIMENTAL INVESTIGATION

The experimental apparatus is shown schematically in Fig. 1. The combustor section consists of a J-47 burner can placed concentrically in a 0.30m diameter by 0.77m long flow duct. The combustor section is followed by a 0.38m diameter by 0.76m long spool piece. This section is followed by a 0.30m diameter by 0.1m long flow duct.

The measurements discussed herein were made at an exit temperature of 920 K and at air mass flow rates of 0.5, 1.13, and 1.68 kg/sec. The corresponding velocities at the exit of the long duct were 18.5, 41.6, and 61.3 m/sec and the corresponding fuel flow rates were 0.009, 0.018, and 0.027 kg/sec. The fuel used was Jet A.

Simultaneous internal fluctuating pressure measurements were made at the three locations shown in Fig. 1. The transducers used ere conventional 5/8 cm diameter (nominal) pressure response condenser microphones. To avoid direct exposure to the severe environment within the flow duct, the microphones were mounted outside the duct and the fluctuating pressure in the duct was communicated to the transducers by "semi-infinite" acoustic waveguides. More information on the probes is given in reference (2).

Constant-bandwidth pressure auto-spectra measured at three test conditions are shown in Fig. 2. The spectra measured in the spool piece upstream of the area contraction are shown in Fig. 2(a). The spectra measured near the entrance to the long duct downstream of the area contraction are shown in Fig. 2(b). The structure of the spectra shown in Figs. 2(a) and 2(b) does not change greatly with operating condition over the frequency range from 2 to 200 Hz. Also the location of resonance peaks and dips in Figs. 2(a) and 2(b) is nearly the same for each operating condition. Moreover, the peaks tend to be sharper at the low frequencies and more broad at the higher frequencies. However, the spectra shown in Fig. 2(a) have a different structure than those shown in Fig. 2(b).

Constant bandwidth pressure cross-spectra measured across the area contraction at three test conditions are shown in Figs. 3(a), 3(b), and 3(c), respectively. Both magnitude and phase are shown. The location of the resonance peaks and dips in the magnitude plot of the cross spectra is nearly the same at each test condition. Also, the peaks tend to be sharper at the low frequencies and more broad at the higher frequencies. The phase plot cannot be characterized as either just a negative sloped straight line due to a time delay nor just a curve that varies abruptly between 0 and 180 degrees in a regular manner that would be due to the presence of waves having approximately equal magnitude but opposite sign travelling upstream and downstream. Instead the phase plot shows both tendencies with the time delay tendency dominating at the higher frequencies.

A large peak appears above 200 Hz in the spectra measured at 41.6 m/sec and at 61.3 m/sec. These peaks appear at such high frequencies that they cannot be related to specific duct resonance harmonics. The peaks may be due to a feedback resonance between the combustor and the duct. They are not analyzed in this paper.

COMPARISON WITH EXPERIMENTAL DATA

Results determined by employing the model using $\tau_s/\kappa_s = 1.0$ and $\tau_s/\kappa_s = 0.001$ are shown in Figs. 4 to 7. Exhibited in Fig. 4 is the sound propagation velocity and the attenuation. For $\tau_s/\kappa_s = 1.0$ the attenuation is zero and the sound propagation velocity is equal to the adiabatic speed of sound. However, for $\tau_s/\kappa_s = 0.001$ the attenuation is greater than 0.5 dB from 50 to 320 Hz and the sound propagation velocity varies from 508 to 580 m/sec.

The auto-spectra and cross-spectra calculated for $\tau_s/\kappa_s = 1.0$ and $\tau_s/\kappa_s = 0.001$ are compared with the data measured at $v = 18.5$ m/sec in Figs. 5 to 7. The model calculations made using $\tau_s/\kappa_s = 1.0$ produce results which do not agree with the data. However, the calculated auto-spectra appear to be stretched out versions of the measured auto-spectra.

The model calculations of pressure auto-spectra and cross-spectra made using $\tau_s/\kappa_s = 0.001$ show better agreement with the measured data. The peaks and dips in the calculated pressure auto-spectra and cross-spectra are closer to the locations of the peaks and dips in the measured data. In addition, the structure of the measured and calculated curves is similar.

DISCUSSION

The large discrepancy between the auto-spectra calculated using the model with $\tau_s/\kappa_s = 1.0$ (no attenuation and a sound propagation velocity of 610 m/s) and the measured pressure auto-spectra compared in Figs. 5(a) and 6(a) might have two explanations. First, the approach used to model the system might not apply. For example, the dips and peaks in the measured spectra could be due to some complicated feedback interaction process between the combustion noise source and the duct which would not be related to the manner in which sound propagates in the duct. Second, the approach could be correct and the values of attenuation and sound propagation velocity might be in error. The results obtained using the model with

the $\tau_s/k_s = 0.001$ shown in Figs. 5(b) and 6(b) suggest the acoustic model is correct since the characteristic structure of the measured spectra between 2 and 200 Hz is similar to the calculated spectra. However, the best argument for the correctness of the acoustic model is the agreement between the measured and calculated phase angle curves compared in Fig. 7(b) since the cross-spectrum phase angle is independent of the source region. While these results indicate that the acoustic model is correct, they also suggest that a more complex model for the soot particle oxidation process may be necessary. The use of a constant time-independent soot particle temperature greatly over simplifies a complex problem. In addition, the combustor inlet and duct exit boundary conditions used herein may need to be improved.

CONCLUDING REMARKS

The model discussed provides a good method for predicting pressure auto-spectra and cross-spectra at an area contraction. The method depends only on a single parameter.

The results obtained indicate that dispersion and attenuation may be a fairly common occurrence in liquid fuel combustor test facilities. They suggest that it may not be correct to assume that sound propagates adiabatically in combustor test facilities.

The propagation of sound in a combustion duct facility appears to be a complex process. The presence of oxidizing soot particles may be affecting strongly the propagation of sound at combustion noise frequencies. Theoretical analysis of the affect of oxidizing soot particles is in a primitive stage of development. Further theoretical analysis seems warranted. Also, experiments which are designed to ascertain functional dependences that can be checked against theory and which include both acoustic and combustion measurements would be of interest.

REFERENCES

1. Miles, J. H., and Raftopoulos, D. D., "Spectral Structure of Pressure Measurements Made in a Combustion Duct," NASA TM-81471, 1980.

2. Reshotko, M., Karchmer, A., Penko, P. F., and McArdle, J. G., "Core Noise Measurements on a YF-102 Turbofan Engine," AIAA Paper No. 77-21, Jan. 1977.

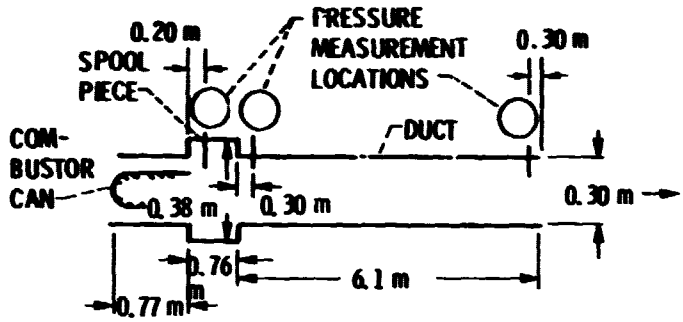

Figure 1. Ducted combustion system.

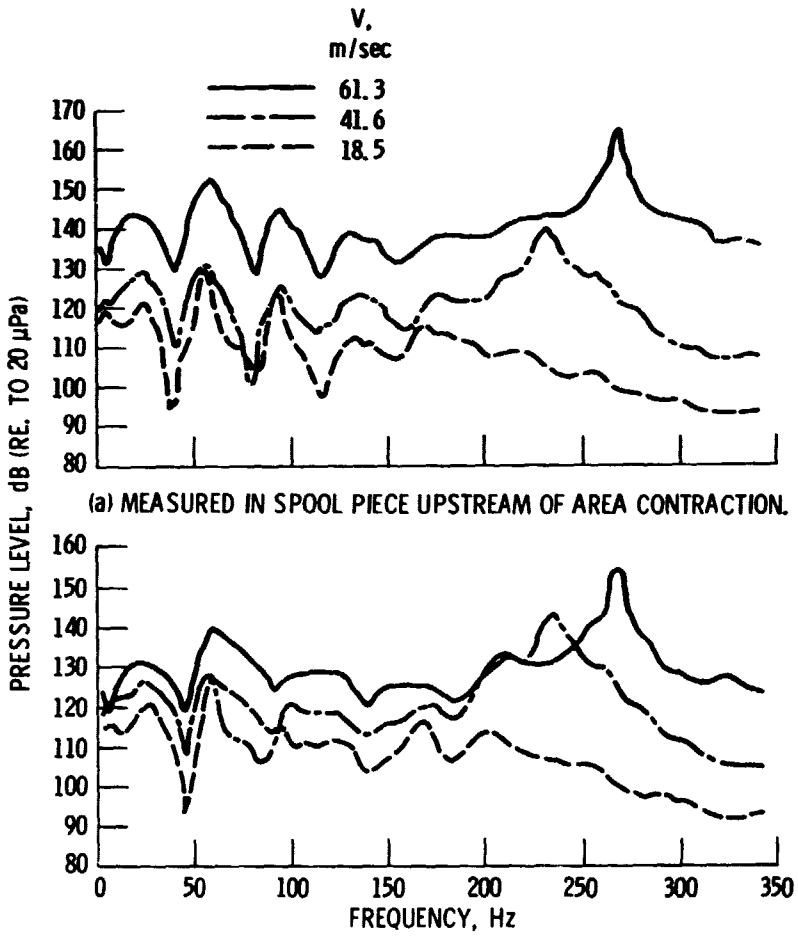

(a) MEASURED IN SPOOL PIECE UPSTREAM OF AREA CONTRACTION.

(b) MEASURED NEAR ENTRANCE TO LONG DUCT DOWNSTREAM OF AREA CONTRACTION.

Figure 2. - Pressure auto-spectra.

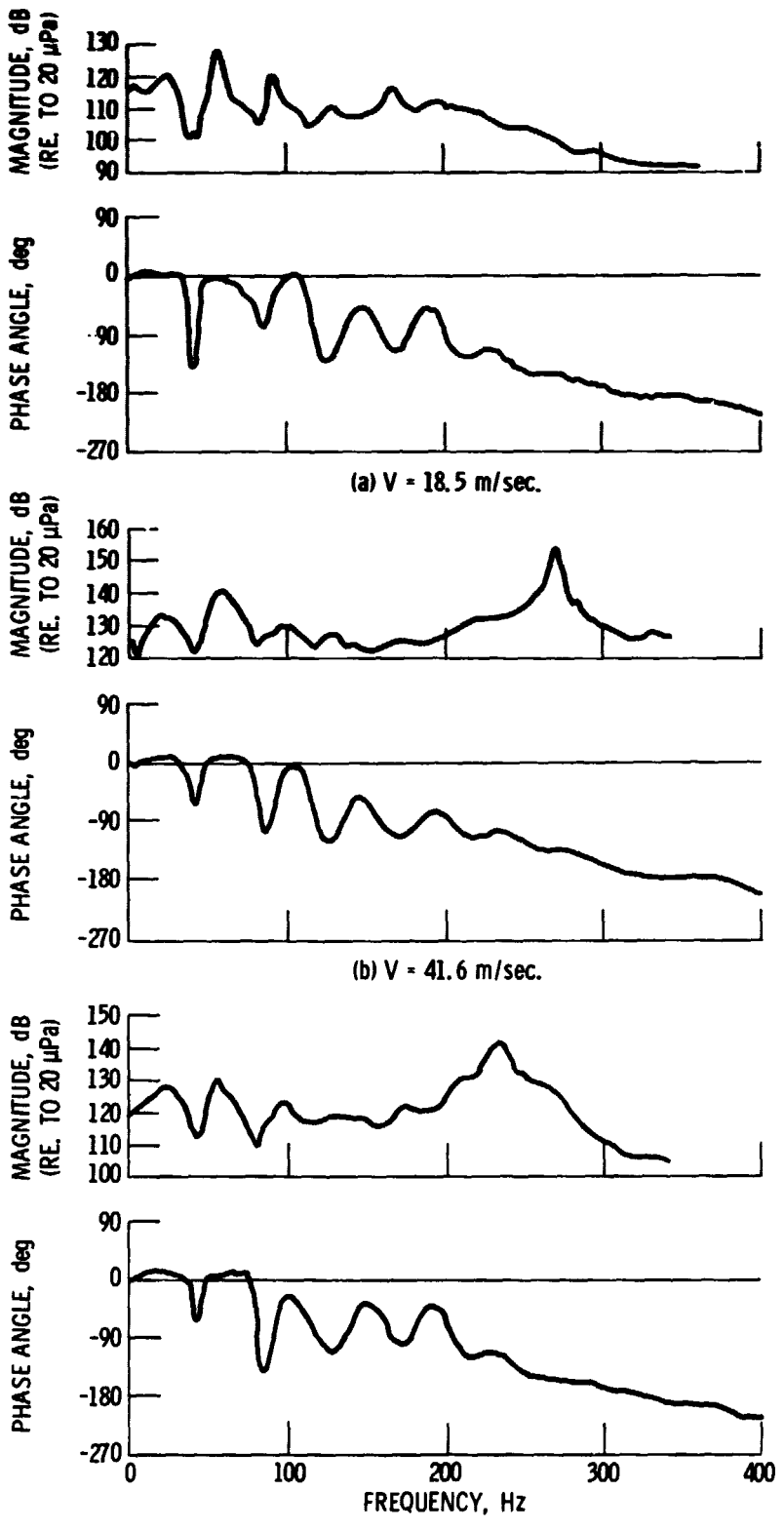

Figure 3. - Measured pressure cross-spectra across area contraction.

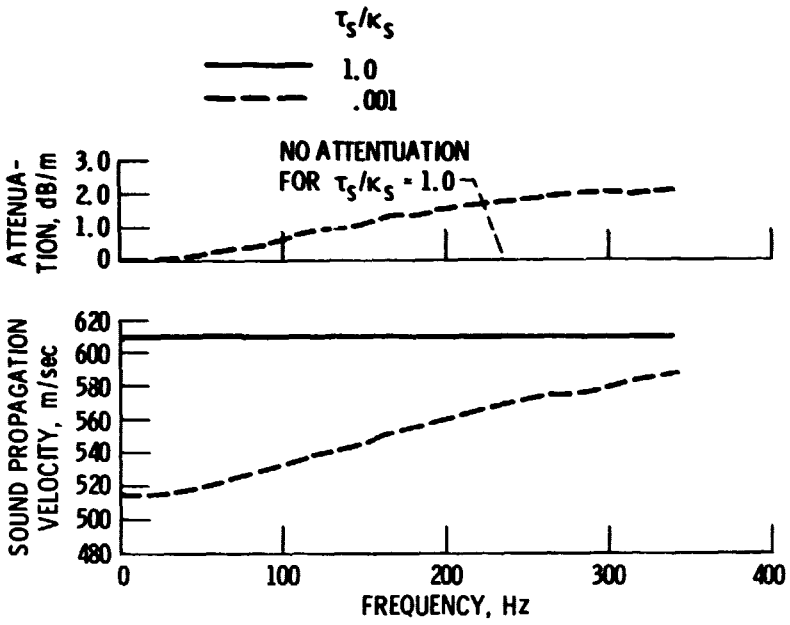

Figure 4. - Sound propagation velocity and attenuation calculated from model.

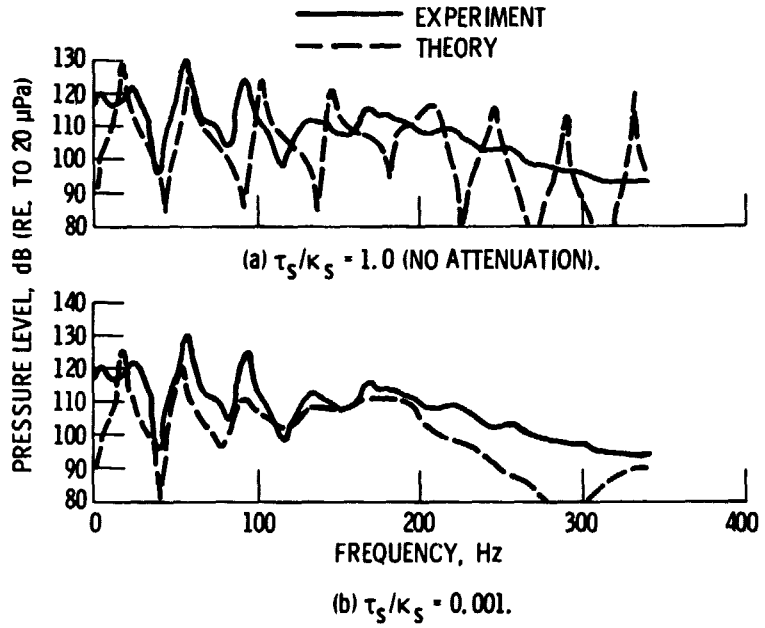

(a) τ_s/κ_s = 1.0 (NO ATTENUATION).

(b) τ_s/κ_s = 0.001.

Figure 5. - Comparison of measured and calculated auto-spectra in spool piece downstream of area contraction (V = 18.5 m/sec).

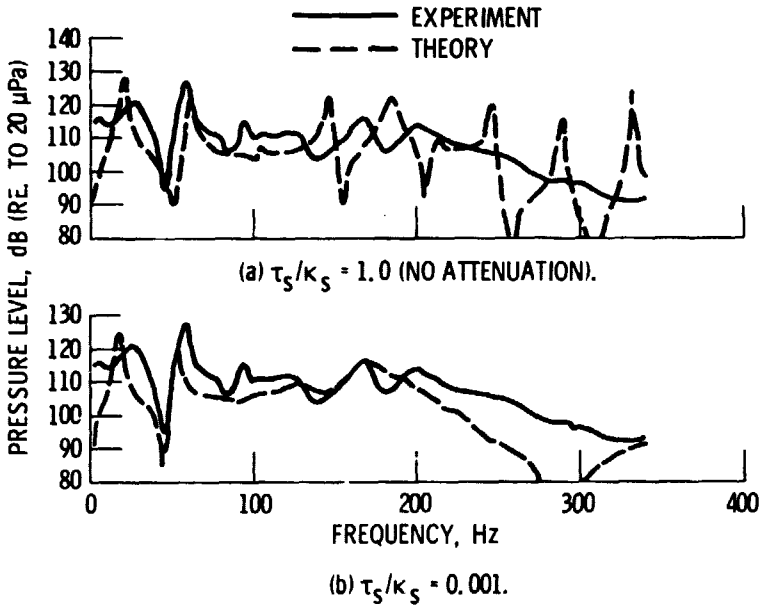

Figure 6. - Comparison of measured and calculated auto-spectra near long duct entrance upstream of area contraction (V = 18.5 m/sec).

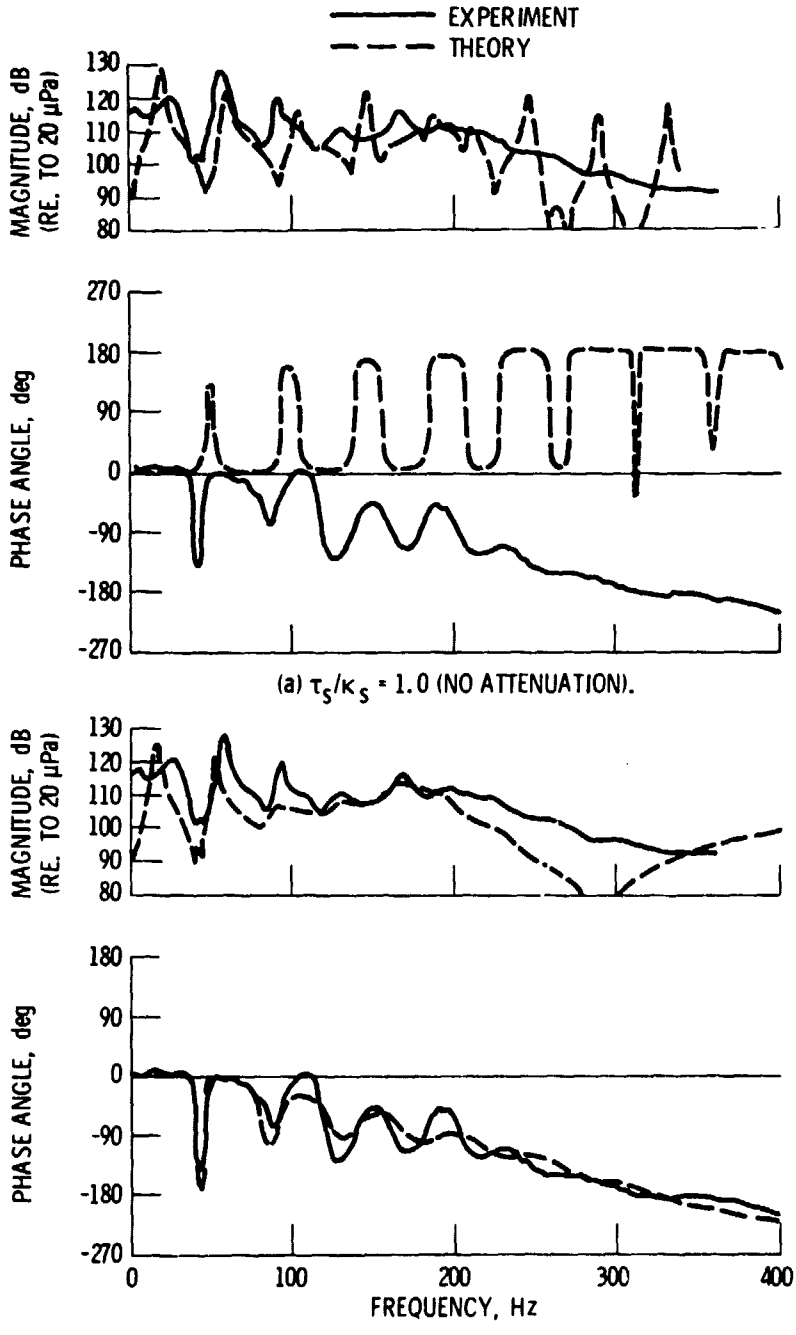

Figure 7. - Comparison of measured and calculated cross-spectrum across area expansion (V = 18.5 m/sec).